https://doi.org/10.48048/tis.2022.4615

Synthesis, Characterisation and Corrosion Inhibition of Mild Steel by Butyltin(IV) 2-Acetylpyridine 4-Methyl-3-Thiosemicarbazone in HCl

Nur Nadira Hazani[1], Nur Nadia Dzulkifli[2,*], Sheikh Ahmad Izaddin Sheikh Mohd Ghazali[2] and Yusairie Mohd[1]

[1]Faculty of Applied Sciences, Universiti Teknologi MARA, Shah Alam, Selangor 40450, Malaysia
[2]School of Chemistry and Environment, Faculty of Applied Sciences, Universiti Teknologi MARA Cawangan Negeri Sembilan, Kampus Kuala Pilah, Pekan Parit Tinggi, Kuala Pilah, Negeri Sembilan 72000, Malaysia

([*]Corresponding author's email: nurnadia@uitm.edu.my)

Received: 11 April 2021, Revised: 24 June 2021, Accepted: 14 July 2021

Abstract

Schiff base ligand, 2-acetylpyridine 4-methyl-3-thiosemicarbazone (Me-LH), and its organotin complex ($BuSn(Me\text{-}LH)Cl_2$) were synthesized, characterized, and subjected to corrosion inhibition study. The spectra and crystal structure obtained revealed that the ligand is coordinated by pyridyl nitrogen, azomethine nitrogen, and thiolate sulfur to organotin (IV) ion. Corrosion inhibition of the synthesized compounds on mild steels in 1 M HCl solution at different concentrations were tested using weight loss, Electrochemical Impedance Spectroscopy (EIS), potentiodynamic polarization, Scanning Electron Microscopy (SEM) and adsorption analyses. Corrosion inhibition results showed that the complex had a strong corrosion inhibitory effect in comparison to the ligand. The inhibition efficiency of all the techniques improved with an increase in the concentration of corrosion inhibitor. Polarization analysis results showed that the compounds can be categorized as mixed-type inhibitors. Meanwhile, the EIS study indicates that with an increase in the concentration of corrosion inhibitor, the resistance to charge transfer increased. This resulted in the adsorption of inhibitors and the development of a protective layer on the mild steel surface which was further confirmed by SEM analysis. The adsorption isotherm of compounds on a mild steel surface followed the Langmuir isotherm model.

Keywords: Organotin (IV), Thiosemicarbazone, Corrosion, EIS, Langmuir isotherm

Introduction

Acids such as hydrochloric acid and sulfuric acid are generally used to discard rust during steel pickling, cleaning and descaling as a part of industrial processes [1-4]. However, the usage of acidic solutions can cause corrosion of metallic materials hence various researches have shown that the addition of corrosion inhibitor in the acidic solution during scale and rust removal process can reduce corrosion [5]. This indirectly will reduce the damage of metallic material. Because of their toxicity and difficulty in disposal, many inorganic inhibitors, particularly those containing phosphate, chromate, and other heavy metals, are now being increasingly limited or prohibited by various environmental protections, especially in the marine industry, where aquatic life is at risk.

The efficacy of corrosion inhibitor depends on the thiosemicarbazone derivatives ability to adsorb and form a layer on the metallic surface. The coating of a metallic surface with thiosemicarbazide derivative enables protection from the effect of aggressive solution [6,7]. Organic compounds consist of nitrogen, oxygen, fur atoms and/or delocalized π-electrons have been reported to be effective corrosion inhibitors typically used in acidic media. Inhibitors with more than one heteroatom, such as nitrogen (N) and sulfur (S) exhibit a better inhibitory effect than individual N or S [8,9]. Thiosemicarbazone possesses N, N, S atoms which when interacting with a metal ion would increase inhibition efficiency.

In addition, the effectiveness of inhibitor increased in the presence of metal ion such as organotin [10,11]. Organotin complexes are generally distinguished by the Sn^{4+} ion bound to one to 4 ligands. In a previous study, complex formation of metal tin (Sn) with thiosemicarbazone derivatives was reported as corrosion inhibitor because organotin is recognized for biocidal, reduced friction and wear, as well as corrosion inhibiting properties [12]. Biocidal characteristic which functions to avoid bio fouling together

with wear and corrosion resistance is an important property for a good corrosion inhibitor [13]. Organotin complex forms the protective layer to the metal surface which is resistant to metal dissolution. The layer formed becomes a sacrificial material which functions as barrier on the metal surface. The development of new organotin complexes with thiosemicarbazone derivatives has initiated new research efforts that go beyond the focus on biological activities such as antimicrobial, antimalarial, anticancer, antifungal, antitubercular and antiviral.

To date, limited studies have been conducted to evaluate the function of organotin ion together with thiosemicarbazone derivatives in inhibiting metallic corrosion. For example, some of tin complexes as corrosion inhibitor are reported reacting organotin ion with thiophenic [14], chlorobenzoates [15], dithiobiurets derivatives [16], dihydroxybenzoate [17] and dinitrobenzoate compounds [18]. In the present study, the combination of butyltin(IV) trichloride with 2-acetylpyridine-4-methyl-3-thiosemicarbazone in a ratio of 1:1 was synthesised as a novel organotin complex, BuSn(Me-LH)Cl_2. The presence of main functional groups, the percentage of elements (C, H, N, S) and the types of electron transition in the Me-LH and BuSn(Me-LH)Cl_2 were determined using a Fourier Transform Infrared-Attenuated Total Reflection (FTIR-ATR), an elemental analyzer (CHNS), and an Ultraviolet-Visible Spectrophotometer (UV-Vis), respectively. Subsequently, the structures of Me-LH and BuSn(Me-LH)Cl_2 were confirmed using a Nuclear Magnetic Resonance (NMR) spectrometer and an X-ray crystallography diffractometer. Additionally, corrosion inhibition performances of both compounds in hydrochloric acid (HCl) were also analysed using the weight loss (theoretical study), electrochemical impedance spectroscopy and potentiodynamic polarisation techniques to determine their efficacy in inhibiting corrosion of mild steel in 1 M HCl at ambient temperature (303 K) at different concentration levels. Lastly, the surface morphology of mild steels was visualized by scanning electron microscopic (SEM) analyses and the Langmuir isotherm was used to determine the adsorption mode of inhibitor on the mild steel surface.

Materials and methods

Material

Chemicals 2-acetylpyridine 4-methyl-3-thiosemicarbazide, butyltin(IV) trichloride and solvents of analytical grade (ethanol, acetic acid, hydrochloric acid) were purchased from Sigma Aldrich. All the reagents were used without further purification. A 2.0×2.5 cm^2 mild steel with a chemical composition of C (0.34 %), Mn (0.76 %), P (0.02 %), Si (0.3 %), and balance % Fe was used for corrosion inhibition study.

Instrumentations

The melting point of Me-LH and BuSn(Me-LH)Cl_2 was measured using a melting point device (SMP10 Stuart). The elemental analysis of the synthesized compounds was performed using an elemental analyser (Thermo Finnigan Flash EA 1112 Series). The infrared spectra were obtained using a Perkin Elmer spectrophotometer while the FT-IR spectra were recorded using the FTIR-ATR. The electronic absorption spectra were acquired using a 1 cm quartz cuvette containing 1×10^{-5} M sample in dimethyl sulfoxide (DMSO) on a PG Instrument T80/T80+ spectrophotometer operating in the wavelength range from 200 to 600 nm. Meanwhile, the ^{1}H and ^{13}C NMR spectra were recorded using the BRUKER spectrophotometer and deuterated DMSO (DMSO-$_{d6}$) was used as a solvent and trimethylsilane (TMS) was utilized as an internal reference. A Bruker Smart APEX CCD diffractometer equipped with a monochromatic graphite Mo-Kα (λ = 0.71073Å) was used to determine the crystal structure of the complex at a temperature of 276 K [19]. Data for Me-LH and BuSn(Me-LH)Cl_2 were collected and reduced using SMART and SAINT program. The molecular designs of both compounds were created using the SHELXTL program and publication material by SHELXTL and PLATON program package [20].

Experimental steps

The Me-LH and BuSn(Me-LH)Cl_2 were prepared by a method as described by Hazani *et al.* 2019 [21]. 2-acetylpyridine 4-methyl-3-thiosemicarbazone (Me-LH) was prepared by combining an ethanolic solution (10 mL) of 4-methyl-3-thiosemicarbazide and ethanolic solution (10 mL) of 2-acetylpyridine. Then, a few drops of glacial acetic acid were added to the mixture. The mixture was then refluxed under continuous stirring at 60 - 70 °C for 2 h, followed by the cooling down of the mixture at room temperature. Slow evaporation was performed to yield crystalline product at room temperature. The crystalline product was then filtered and rinsed with cold methanol and dried over anhydrous silica gel.

The purification of Me-LH was carried out using a thin layer chromatography (TLC) method. For the synthesis of BuSn(Me-LH)Cl_2, the Me-LH was first dissolved in ethanol (10 mL), while the butyltin(IV) trichloride salt was dissolved in distilled water (10 mL). Then, the metal salt solution was added dropwise into the Me-LH solution. After that, the mixture was continuously stirred for 4 h, purified and treated with cold ethanol. The powder formed was dried over the anhydrous silica gel. The BuSn(Me-LH)Cl_2 was recrystallized in the mixture of chloroform and ethanol with a ratio of 1:1.

Corrosion inhibition study

Hydrochloric acid (HCl) solution (1 M) was prepared by diluting 37 % of analytical grade HCl with distilled water. Different concentration levels of the Me-LH and BuSn(Me-LH)Cl_2 were prepared ranging from 0.1 to 1.5 mM. The compounds for each concentration were freshly prepared by dissolving [] in prepared solution of 1 M HCl.

Mild steel weight loss measurement

First, the initial weight of mild steel was weighed using an analytical balance. The specimen was then soaked in 10 mL of 1 M HCl with and without the presence of corrosion inhibitors at varying concentration levels at room temperature. After immersion for 24 h in the acidic solution, the mild steel specimen was rinsed with distilled water and dried at room temperature. The specimen was then weighed and recorded as the final weight. The experiment was operated 3 times and the mean weight was calculated. The weight loss of mild steel, $\Delta W(g)$, corrosion rate C_{RW} ($mgcm^{-2}h^{-1}$), surface coverage (θ) and inhibition efficiency, $IE_{WL}(\%)$ were calculated as shown in Eqs. (1), (2), (3) and (4), respectively [22].

$$\Delta W = W_1 - W_2 \quad (1)$$

$$C_{RW} = \frac{\Delta W}{St} \quad (2)$$

$$\theta = \frac{C°_{RW} - C_{RW}}{C°_{RW}} \quad (3)$$

$$IE_{WL} = \left(\frac{C°_{RW} - C_{RW}}{C°_{RW}} \right) \times 100 \quad (4)$$

W_1 and W_2 are the weight of specimens before and after immersion in acidic solution, respectively. S is the surface area of the mild steel (cm^2), t is the immersion time (h), $C°_{RW}$ and C_{RW} refer to corrosion rates in the absence and presence of inhibitors, respectively.

Electrochemical Measurement

Three conventional electrode cells were used for polarisation and electrochemical impedance spectroscopy (EIS) tests. They were platinum rod, silver-silver chloride (Ag/AgCl) and mild steel which was used as the counter electrode, reference electrode, and working electrode, respectively. The working electrode was developed by implanting mild steel with a surface area of 0.1 cm^2 exposed to epoxy resin. Before usage, the mild steel specimen was polished with a series of 320 to 1,200 grades of silica carbide paper and was then washed with distilled water followed by acetone degreasing. The analysis was performed at room temperature by soaking the working electrode in an unstirred aggressive electrolyte over an open-circuit potential (OCP) for approximately 10 min to achieve equilibrium. The EIS experiments were carried out at a corrosion potential (E_{corr}) with a frequency range from 10 kHz to 0.1 Hz using the peak-to-peak amplitude of 0.01 V at the OCP [23]. The inhibition efficiency, IE_{EIS} (%) was calculated as expressed in Eq. (5) [23].

$$IE_{EIS} = \left(\frac{R°_P - R_P}{R°_P} \right) \times 100 \quad (5)$$

R_P and $R°_P$ correspond to polarization resistances of mild steel in the absence and presence of inhibitor, respectively.

Potentiodynamic polarization or Tafel extrapolation measurements were also performed on the same electrode immediately after the EIS measurement without any mild steel surface treatment [24]. Each test was carried out with 3 replicates per concentration level. The corrosion potentials were recorded at a scanning rate of 0.001 Vs^{-1} in a potential range of ±100 mV [25]. The inhibition efficiency (IE_{POL}) was calculated based on Eq. (6):

$$IE_{POL} = \left(\frac{i^{o}_{corr} - i_{corr}}{i^{o}_{corr}} \right) \times 100 \quad (6)$$

where, i°_{corr} and i_{corr} correspond to current density with the absence and presence of inhibitor, respectively.

Evaluation of mild steel surface morphology using a scanning electron microscope

Surface morphologies of mild steel specimens before and after immersion in an acidic solution for 24 h with and without the existence of 1.5 mM of inhibitors were captured using a Tabletop Electron Microscope (Hitachi TM3030Plus). The energy used for the acceleration beam was 20 kV. All micrographs were taken at a magnification of 5000x and with a scale of 20 µm.

Adsorption isotherm and thermodynamic calculation

It was assumed that adsorption of the inhibitor on mild steel was an integral part of the mechanism of corrosion inhibition. To classify the adsorption mode, different adsorption isotherms such as the Langmuir, Frumkin, and Temkin models were used to measure the degree of surface coverage (θ) by the inhibitor. Of the 3 adsorption isotherms evaluated, the Langmuir adsorption isotherm best suits the inhibitor's adsorption activity, where the linear regression coefficient (R^2) was close to 1. The Langmuir isotherm is expressed in the following Eq. (7).

$$\frac{C}{\theta} = \frac{1}{K} = +C \quad (7)$$

The symbol θ is the metal steel surface coverage, C refers to the concentration of inhibitor and K is the adsorption-desorption equilibrium constant. The thermodynamic Gibb's free energy of adsorption (ΔG_{ads}) equation was used to determine the adsorption in this study [26]. The ΔG_{ads} on the mild steel surface was calculated based on the following Eq. (8) [27].

$$\Delta G_{ads} = -RT \ln (55.5\ K_{ads}) \quad (8)$$

The ΔG_{ads} refers to the free energy of adsorption, R corresponds to the universal gas constant (R = 8.31446 $JKmol^{-1}$), T is the temperature of solution (K), the factor 55.5 is the molar concentration of water (mol/L), and K_{ads} refers to the equilibrium constant that was determined from the intercept of a straight line on the C/θ axis of the Langmuir plot.

Results and discussion

Physicochemical properties of Me-LH and BuSn(Me-LH)Cl_2

The elemental analysis data of Me-LH and BuSn(Me-LH)Cl_2 were consistent with the predicted structures and molecular formula. The melting point of BuSn(Me-LH)Cl_2 was found to be higher than Me-LH which signified successful complex formation. The measured molar conductivity of BuSn(Me-LH)Cl_2 ranged from 12 to 20 $ohm^{-1}cm^2mol^{-1}$ which further affirmed that the complex is of a non-electrolyte behavior with the BuSn(Me-LH)Cl_2 found to be in 1:1 metal to ligand ratio [28]. Physical properties and data analysis of Me-LH and BuSn(Me-LH)Cl_2 are depicted in **Table 1**.

Table 1 Physical properties and data analysis of Me-LH and BuSn(Me-LH)Cl_2 compounds.

Compound	Percentage Yield (%)	Colour	Melting Points (°C)	Molar Conductivity ($Scm^2.mol^{-1}$)	Elemental Analysis (Experimental) (%)			
					C	H	N	S
Me-LH	71.61	Light yellow	176 - 177	-	51.56 (51.92)	5.88 (5.77)	28.06 (26.92)	14.55 (15.38)
BuSn(Me-LH)Cl_2	89.27	Yellow	222 - 225	17.1	34.78 (34.39)	4.41 (4.44)	12.11 (12.34)	7.91 (7.06)

Determination of functional groups present in the Me-LH and BuSn(Me-LH)Cl_2 compounds using a FTIR-ATR

The infrared spectra for the ligand and complex are presented in **Figure 1**. The Me-LH exists in a solid-state which is in the form of thione as confirmed by the absence of a stretching band around 2,500 - 2,650 cm^{-1} which represents thiol group, ν(S-H) [29]. The presence of bands representing ν(C=S) at 1,074 cm^{-1} and ν(N-H) at 3,240 cm^{-1} verified that the Me-LH exists in a thione form [30,31]. It was also noted that the stretching bands of imine group, ν(C=N) and imine pyridine group, ν(C=N_{py}) for the BuSn(Me-LH)Cl_2 sample shifted to lower wavenumbers at 1,511 and 1,560 cm^{-1}, respectively. These findings indicated that the azomethine N and pyridine N coordinate with the Sn(IV) ion. Upon the complexation, the ν(N-H) disappeared due to thioenolisation of C=S [32]. Furthermore, the stretching band of ν(C=S) disappeared for BuSn(Me-LH)Cl_2 sample but a stretching band ν(C-S) was found at 1,049 cm^{-1}. This could be explained by the coordination that occurred after enolisation of C=S accompanied by the deprotonation of sulfur by thiolate sulfur (CS^-) [33]. Nevertheless, the coordination between C=N_{py}, C=N, and CS^- atoms from the Me-LH to the Sn(IV) ion can be ascribed to the presence of new stretching bands such as ν(Sn-N_{py}) ν(Sn-N) and ν(Sn-S) at 285, 321 and 356 cm^{-1}, respectively [34]. Additionally, a stretching band of ν(Sn-Cl) was also noted at 250 cm^{-1} [35].

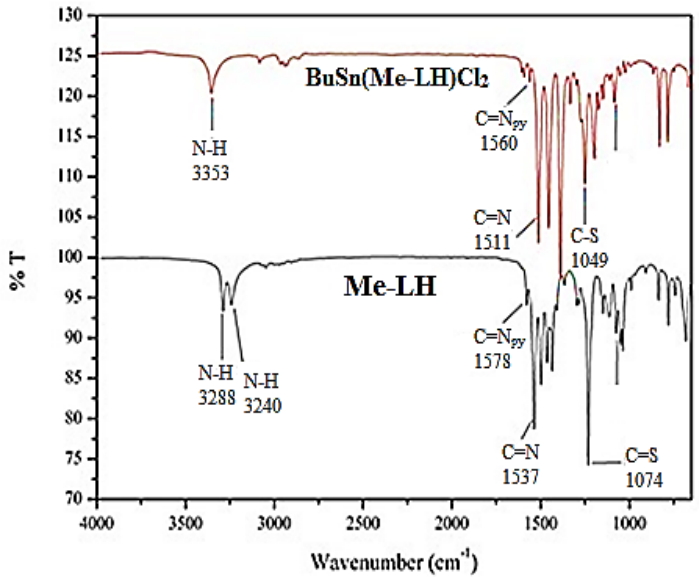

Figure 1 Infrared spectra for Me-LH and BuSn(Me-LH)Cl_2.

Determination of electron transition in the Me-LH and BuSn(Me-LH)Cl_2 compounds using a UV-Vis

UV-Vis absorption data for the Me-LH and BuSn(Me-LH)Cl_2 compounds are reported in **Table 2**. The UV-Vis absorption spectra are shown in **Figure 2**. Me-LH showed an absorption peak at 320 nm where it was appointed as π→π* transition. The peak correlated to the electron transition in the C=N moiety. Meanwhile, absorption peak ascribed to n→π* transition could not be detected in the Me-LH

spectrum. This could be due to stronger absorption of π →π* transition which might have overshadowed the n→π* transition [36]. Upon complexation, the hypsochromic shift of π→π* transition was drifted to a shorter wavelength that showed donation of electron lone pair from N or S atom to metal ion [37]. A new absorption peak was also noted at 396 nm which was assigned to the ligand to metal charge transfer (LMCT) [38]. The transition was attributed to the transfer of electrons from the lone pair of a nitrogen atom to the empty metal ion orbital (N→Sn) [39]. The change of π→π* transition shifting and the presence of LMCT peak further supported the coordination of ligand to Sn(IV) ion.

Table 2 UV-Vis data of Me-LH and BuSn(Me-LH)Cl_2 compounds.

Compound	Transition	λ_{max}(nm)	Maximum absorbance, ε ($M^{-1}cm^1$)
Me-LH	π→π*	320	65,400
BuSn(Me-LH)Cl_2	π→π*	301	65,400
	LMCT	396	89,300

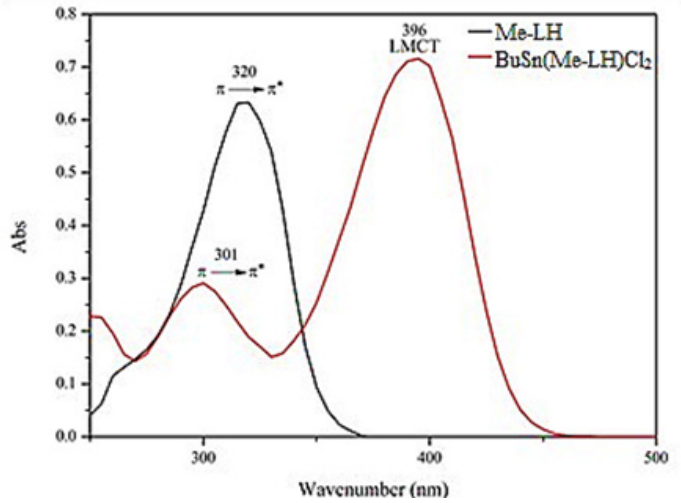

Figure 2 UV-Vis absorption spectra for Me-LH and BuSn(Me-LH)Cl_2.

^{1}H, ^{13}C and ^{119}Sn NMR spectra data of Me-LH and BuSn(Me-LH)Cl_2

Table 3 shows the ^{1}H and ^{13}C NMR spectra data of Me-LH and BuSn(Me-LH)Cl_2 compounds. The Me-LH exhibited a resemblance of thione structure as supported by the absence of a characteristic broad signal at 4.0 ± 0.2 ppm representing thiol, SH resonance [40]. The ^{1}H NMR of BuSn(Me-LH)Cl_2 showed a considerable variation in chemical shift of the Me-LH where coordination with the Sn(IV) ion has been proven. Upon complexation, the signal of 2° N(1)H [Me-LH] shifted to downfield and the 2° N(2)H [Me-LH] signal vanished due to deprotonation process as a result of coordination to the Sn(IV) ion. On the contrary to the Me-LH, CH_3-C=N signal of BuSn(Me-LH)Cl_2 shifted downfield which indicated the role of C=N in coordination to the Sn(IV) ion. In a previous study, multiplet signals of aromatic ring proton were reported to shift downfield upon complexation [41]. The butyl group that was attached to the Sn(IV) ion showed signals between 0.95 and 2.06 ppm. In ^{13}C NMR of Me-LH, the signals of C=N and C=S appeared at 155.22 and 179.10 ppm, respectively. However, the signals shifted upfield in the BuSn(Me-LH)Cl_2 which indicated that the coordination with the Sn(IV) ion occurred through sulfur and nitrogen atoms of the pyridine group. The presence of additional signals was related to butyl group that was linked to the Sn(IV) ion [42,43]. The ^{119}Sn NMR is recognized for verification of Sn(IV) ion responsible for coordination number and bonding details [44]. At –343.68 ppm, the ^{119}Sn NMR spectrum displayed a signal that suggested the presence of 1 tin site. The variation in the ^{119}Sn chemical shifts was reported to depend on the number of the alkyl group and the type of ligand linked to the Sn(IV) ion [45]. Meanwhile,

the position of the ^{119}Sn signal was consistent with the reported range of chemical shifts within –210 to –400 ppm, suggesting a 6-coordinated environment [46].

Table 3 ^{1}H and ^{13}C NMR data of Me-LH and $BuSn(Me\text{-}LH)Cl_2$ compounds.

Compound	Type of proton	Number of proton/multiplicities	Chemical shift, δ (ppm)	Type of carbon	Chemical shift, δ (ppm)
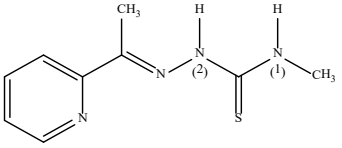 Me-LH	-CH_3	3H / duplet	3.05	-CH_3	31.63
	N(1)H	1H / quartet	8.62	C=S	179.10
	N(2)H	1H / singlet	10.25	C=N	155.22
	CH_3-C=N	3H / singlet	2.38	CH_3C=N	12.56
	Aromatic	4H / multiplet	7.37 - 8.59	Aromatic	121.24 - 148.93
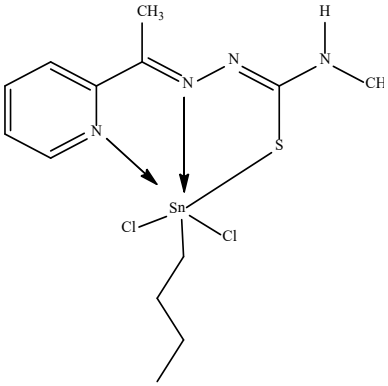 $BuSn(Me\text{-}LH)Cl_2$	-CH_3	3H / duplet	2.99	-CH_3	36.18
	N(1)H	1H / quartet	8.85	C-S	169.77
	CH_3–C=N	3H / singlet	2.72	C=N	145.10
	Aromatic	4H / multiplet	7.88 - 8.52	CH_3C=N	115.13
	Butyl	9H / multiplet	0.95 - 2.06	Aromatic	125.63 - 143.50
				Butyl	25.50- 29.53

X-ray crystallographic study of Me-LH and $BuSn(Me\text{-}LH)Cl_2$

The crystallographic data of the synthesized Me-LH and $BuSn(Me\text{-}LH)Cl_2$ are shown in **Table 4**. The crystal of Me-LH as shown in **Figure 3** has a triclinic P-1 space group with Z = 2. A maximum deviation of 0.008 Å was noted for the C(8) atom from the least square plane, where the pyridine ring fragments (N4/C5/C6/C7/C8/C9) were planar. Meanwhile, both the pyridine ring and the thiourea fragment were co-planar with the dihedral angle between the azomethine fragment of 10.39° and 17.25°, respectively. The thiourea fragment and the pyridine ring were in a trans-configuration representing imine C3=N3. The C2-S1 bond distance found in this study was 1.5284 Å which was close to the value for C=S double bond at 1.56 Å [47]. The $BuSn(Me\text{-}LH)Cl_2$ compound as shown in **Figure 4** was formed by the coordination of Me-LH to Sn(IV) ion which involved thiol sulfur (S), azomethine nitrogen (N) and pyridine nitrogen (N), with the coordination number of tin(IV) moiety equivalent to 6. The complex was crystallized into a triclinic system P-1 space group with Z = 2 resulting in a distorted octahedron structure that can be further confirmed by the bond angle deviation from perfect octahedral geometry of 90°. The largest bond angle for the tin(IV) atom was Cl1-Sn1-Cl2 [166.88°] and it was found that the other atoms that subtended at the tin atom also deviated from the ideal value ranging from 71.65° to 150.65°. The bond length of Sn-N1 [2.1974 Å] and Sn-N2 [2.2069 Å] were close to the sum of covalent radii of Sn-N (2.15 Å). However, the bond lengths were slightly lower than the sum of the Van der Waals radii (3.75 Å) [48] which suggested that the pyridine nitrogen and azomethine nitrogen were bonded to the Sn(IV) ion. Interestingly, the bond length of Sn-N1 was found to be shorter than the Sn-N2 which showed stronger coordination of the azomethine nitrogen than the pyridine nitrogen to the tin atom. Meanwhile, the Sn1-C10 bond length was found to be 2.1386 Å which was slightly shorter than the reported non-polar covalent radii of Sn and C (2.17 Å). Nevetheless, this value is in an acceptable range with other reported organotin complexes [48]. The bond length of Sn1-S1 [2.4989 Å] was found to be longer than the sum of the covalent radii (2.42 Å) which was considerably shorter than the van der Waals radii (4.0 Å) [49]. This showed that the S atom was coordinated to the Sn(IV) ion in the thiolate form resulting in the formation

of Sn-S bond. Furthermore, the bonding of thiolate sulfur to the Sn atom upon complexation was supported by the value of S1-C8 bond length (1.7801 Å) which was close to the range of C-S bond value [50]. Similar findings were also reported by Pérez-Rebolledo *et al.* [51] and Batten [52] where C-S bond length was found to be longer in the complex as compared to the ligand.

Table 4 Crystallographic Data for Me-LH and BuSn(Me-LH)Cl_2 compounds.

	Me-LH	**BuSn(Me-LH)Cl_2**
Formula	$C_9H_{12}N_4S$	$C_{13}H_{20}Cl_2N_4SSn$
Formula weight	208	454.50
The wavelength, Mo Kα (Å)	0.71076	0.71073
Crystal system	Triclinic	Triclinic
Space group	P-1	P-1
a (Å)	7.723(3)	7.8975(8)
b (Å)	8.824(3)	12.0093(12)
c (Å)	15.612(7)	19.781(2)
α (°)	106.104(18)	76.106(7)
β (°)	90.056(17)	79.695(7)
γ (°)	90.066(17)	86.124(7)
Volume (V) (Å^3)	1022.1(7)	1791.2(3)
Z	2	2

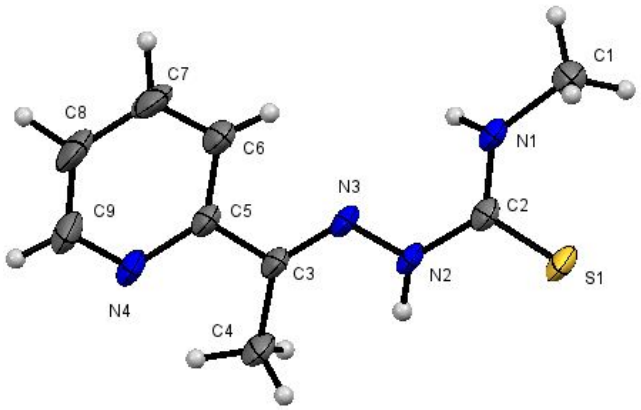

Figure 3 Thermal ellipsoidal plot of Me-LH.

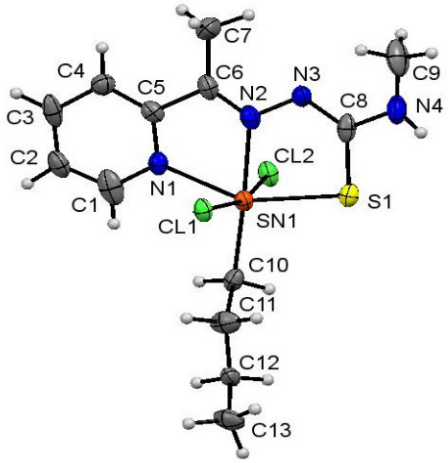

Figure 4 Thermal ellipsoidal plot of BuSn(Me-LH)Cl_2.

Corrosion inhibition study

Weight loss of mild steel

Table 5 shows the weight loss data of mild steel exposed to 1 M HCl in the presence and absence of inhibitors at different concentration levels. The inhibition efficiency increased with an increment in the concentration of corrosion inhibitor. The greater inhibition efficiency of BuSn(Me-LH)Cl_2 was attributed to its higher adsorptive capability. The presence of additional active sites on the complex and the contributory impact of the complex increased size and molecular weight would explain this [53]. These factors caused the build-up of a protective film of adsorbed molecules on the mild steel surface which lowered the corrosive effect of the acidic environment.

Table 5 Weight loss data of metal steels exposed to 1 M HCl with different concentration of Me-LH and BuSn(Me-LH)Cl_2.

Inhibitor	Concentration (mM)	ΔW	CR (mg.cm^{-2}h^{-1})	θ	IE_{WL}(%)
Blank	1 M	0.177	1.475×10^{-3}	-	-
Me-LH	0.1	0.0216	1.800×10^{-4}	0.8658	86.58
	0.5	0.0200	1.667×10^{-4}	0.8870	88.70
	1.0	0.0198	1.650×10^{-4}	0.8881	88.81
	1.5	0.0193	1.608×10^{-4}	0.8907	89.10
BuSn(Me-LH)Cl_2	0.1	0.0063	5.250×10^{-5}	0.9644	96.44
	0.5	0.0059	4.917×10^{-5}	0.9666	96.66
	1.0	0.0048	4.000×10^{-5}	0.9729	97.29
	1.5	0.0033	2.750×10^{-5}	0.9814	98.14

Corrosion inhibition performance measured using electrochemical impedance spectroscopy (EIS)

Table 6 presents the values acquired from the EIS analysis when different concentrations of inhibitors were used. **Figures 5** and **6** portray the Nyquist plots of mild steel in 1 M HCl in the absence and the presence of Me-LH and BuSn(Me-LH)Cl_2, respectively. It can be interpreted from the Nyquist plots that the pattern of impedance curves was not affected by the inhibitors [54]. It should be noted that the Nyquist plots displayed a divergence from the ideal semicircles that could be due to frequency dispersion affected by non-homogeneity or roughness of metal surface during metal dissolution [55,56]. The impedance spectra also showed that the semicircle and the diameters incremented with an increase in the concentration of inhibitors. However, no significant trend in the constant phase element (CPE) parameters, Y0 and n values were observed. The increment in the diameter of the semicircle can be associated with the adsorption of inhibitors on the mild steel surface which improved the efficiency of corrosion inhibition. The inhibitors prevented metal dissolution in 1 M HCl solution with the development of a protective film on the surface of mild steel. The increasing pattern of Rp values implied that the metal/electrolyte interfaces had more inhibitor molecules adsorbed at higher concentrations. Not only that, but it was reported that a larger value of Rp may indicate a slower corrosion rate due to strong inhibition [57]. The most effective inhibitor was found to be the BuSn(Me-LH)Cl_2 at 1.5 mM with 94.05 % of inhibition efficiency based on the impedance measurement.

Table 6 Corrosion inhibition performance of Me-LH and BuSn(Me-LH)Cl_2 for mild steels immersed in HCl.

Inhibitor	Concentration (mM)	Y0 (μF cm^{-2})	n	Rs (ohm cm^2)	Rp (ohm cm^2)	IE_{EIS} (%)
Blank	-	172	0.788	0.59	63.00	-
Me-LH	0.1	64.7	0.901	0.49	117.0	46.15
	0.5	64	0.888	0.16	135.7	53.57
	1.0	79.8	0.875	0.32	155.2	59.41
	1.5	89.2	0.857	0.52	181.7	65.33
BuSn(Me-LH)Cl_2	0.1	53.6	0.995	1.16	638.7	90.14
	0.5	28	0.997	0.39	704.2	91.05
	1.0	24.1	0.997	1.44	830.2	92.41
	1.5	43.6	0.995	0.96	1058.2	94.05

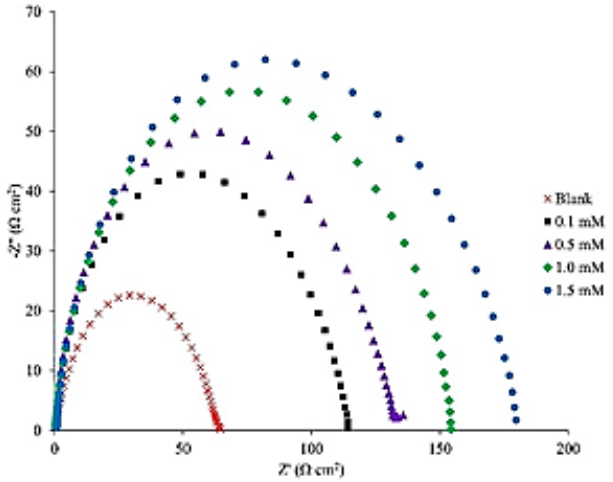

Figure 5 Nyquist plot in the absence and presence of Me-LH at various concentration levels.

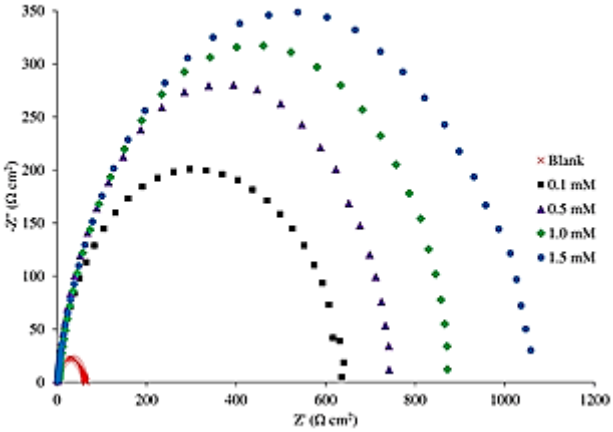

Figure 6 Nyquist plot in the absence and presence of BuSn(Me-LH)Cl_2 at various concentration levels.

Polarisation measurement

The values obtained from the potentiodynamic polarisation curve (Tafel extrapolation) for different concentrations of inhibitors are tabulated in **Table 7**. The parameters evaluated were corrosion current density (i_{corr}), corrosion potential (E_{corr}), anodic Tafel slope (β_a), cathodic Tafel slope (β_c), corrosion rate (CR), and inhibition efficiency (IE_{POL}%) for the mild steel in 1 M HCl with and without inhibitors. **Figures 7** and **8** exhibit the Tafel polarisation curves for mild steel in 1 M HCl solution with and without the presence of inhibitors for Me-LH and BuSn(Me-LH)Cl_2, respectively. The polarisation curves are presented in the plot of E versus log i which provided information such as Tafel slopes, β_a and β_c. Polarisation measurements unveiled that the compounds were the mixed type of inhibitors since their displacement of E_{corr} against the blank was less than 85 mV [58]. The inconsistent trend was observed for the E_{corr} values in the present study. The maximum displacement was 53.76 mV concerning blank which suggested the mixed type nature of the inhibitors. This finding also showed that through anodic and cathodic reactions, corrosion of mild steel was simultaneously inhibited by the inhibitors. This was achieved by the reduction of anodic dissolution and the slower reaction of hydrogen evolution [59]. However, Me-LH primarily suppressed the cathodic reaction that can be related to the shift of E_{corr} to a more negative potential while the BuSn(Me-LH)Cl_2 primarily suppressed the anodic reaction [60]. With an increment in the concentration of inhibitor, the i_{corr} values decreased [61]. When the inhibitors were adsorbed on the mild steel surface, successful corrosion inhibition activity of mild steel in the presence of acidic solution was noted [62,63]. The optimal efficiency of corrosion inhibition according to polarization result was 97.91 % at 1.5 mM of the BuSn(Me-LH)Cl_2.

Table 7 Polarisation data of Me-LH and BuSn(Me-LH)Cl_2 in HCl.

Inhibitor	Concentration (mM)	i_{corr} ($\mu A/cm^2$)	E_{corr} (mV)	β_a (mV/dec)	$-\beta_c$ (mV/dec)	CR (mm/yr)	θ	IE_{pol} (%)
Blank	-	330.64	–423.65	156.53	71.916	3.842	-	-
Me-LH	0.1	157.52	–477.41	178.21	62.773	1.8304	0.5236	52.36
	0.5	129.84	–463.57	199.96	58.31	1.5087	0.6073	60.73
	1.0	122.38	–475.57	152.37	67.424	1.422	0.6299	62.99
	1.5	96.707	–474.66	148.32	58.053	1.1237	0.7075	70.75
BuSn(Me-LH)Cl_2	0.1	14.33	–392.09	129.45	25.877	0.16651	0.9567	95.67
	0.5	10.619	–405.21	79.068	35.713	0.12339	0.9679	96.79
	1.0	10.481	–403.39	70.469	26.452	0.12179	0.9683	96.83
	1.5	6.8963	–400.13	54.354	33.178	0.08014	0.9791	97.91

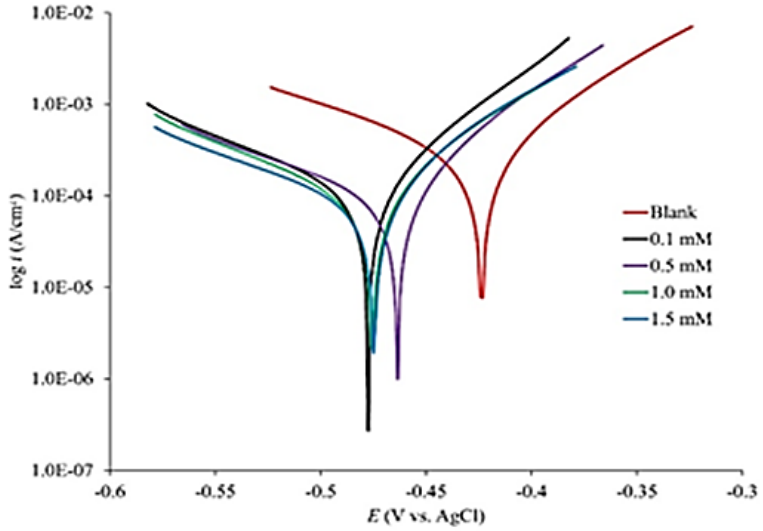

Figure 7 Polarisation curve with and without the addition of Me-LH at different concentration levels of hydrochloric acid.

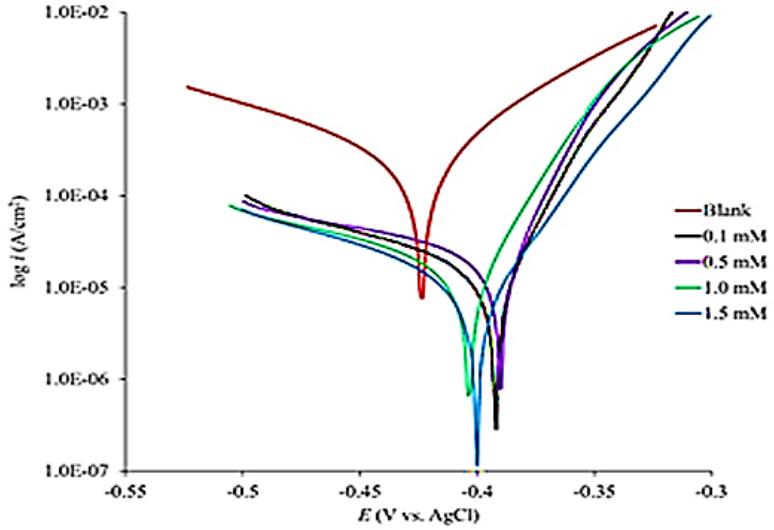

Figure 8 Polarisation curve with and without the addition of BuSn(Me-LH)Cl_2 at different concentration levels of hydrochloric acid.

Adsorption isotherm and thermodynamic study

The adsorption parameter values for both inhibitors are presented in **Table 8** using the 3 methods (WL, EIS, POL) which were deduced from the Langmuir adsorption isotherm. To investigate the form of adsorption mechanism of the inhibitors on mild steel, adsorption isothermal analysis was carried out. The best adsorption isotherm among the Langmuir, Temkin and Frumkin models were selected based on the regression coefficient (R^2) [64]. The best-fit isotherm of this study was the Langmuir isotherm. The adsorption parameter values for both inhibitors are presented in Table 8 using the 3 methods (WL, EIS, POL) which were deduced from the Langmuir adsorption isotherm. **Figures 9 - 11** represent the Langmuir isotherm plots by weight loss, EIS and Tafel extrapolation method, respectively. The $R^2 \approx 1$ value provided by the straight line of the plots verified the suitability of the Langmuir isotherm for the corrosion inhibition analysis. The isothermal findings of the 3 methods of both inhibitors suggested that the inhibitors were adsorbed by monolayer and a mixed adsorption mechanism on the mild steel surface. It was assumed that the mild steel surface can adsorb 1 species per adsorption site according to the Langmuir isotherm model. This may be clarified by the fact that only a fixed number of adsorbed species have access to the adsorption site and there is no interaction with other adsorbed species [65]. Moreover, in this study, the thermodynamic analysis was also performed by calculating the standard free adsorption energy (ΔG_{ads}) to understand the adsorption mechanism [66]. **Table 9** shows the ΔG_{ads} values for categorization of mechanism type.

Table 8 Langmuir adsorption isotherm data of Me-LH and $BuSn(Me\text{-}LH)Cl_2$ compounds.

Inhibitor	Method	R^2	Slope	K_{ads} (M^{-1})	ΔG_{ads} (kJ/mol)
Me-LH	WL	1	1.120	333.3×10^3	–41.46
	EIS	0.993	1.481	7.462×10^3	–32.05
	POL	0.999	1.37	15.15×10^3	–33.80
$BuSn(Me\text{-}LH)Cl_2$	WL	1	1.017	200.0×10^3	–40.19
	EIS	0.999	1.06	83.333×10^3	–38.02
	POL	0.999	1.02	200.0×10^3	–40.19

Table 9 Type of inhibitor mechanism.

Type of inhibitor	Chemisorption	Physisorption	Mixed
Value	−40 kJ mol^{-1} or more negative	−20 kJ mol^{-1} or less negative	between –20 to –40kJ mol^{-1}

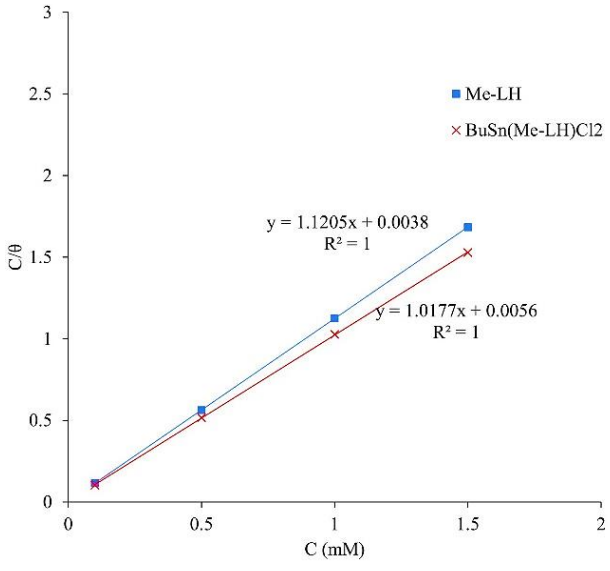

Figure 9 Langmuir isotherm for the adsorption of inhibitors using the weight loss method.

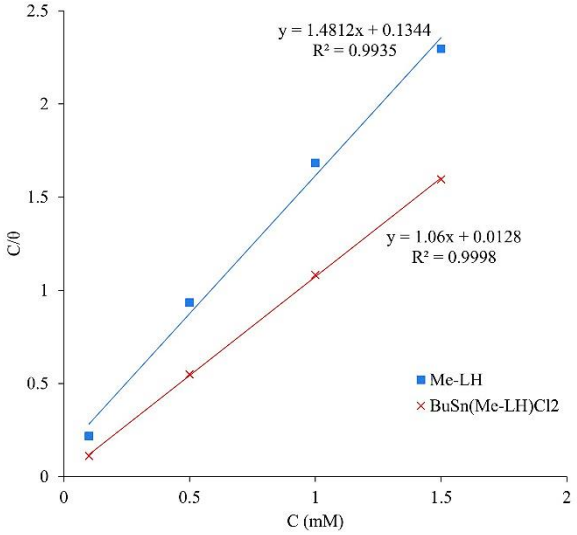

Figure 10 Langmuir isotherm for the adsorption of inhibitors using the EIS method.

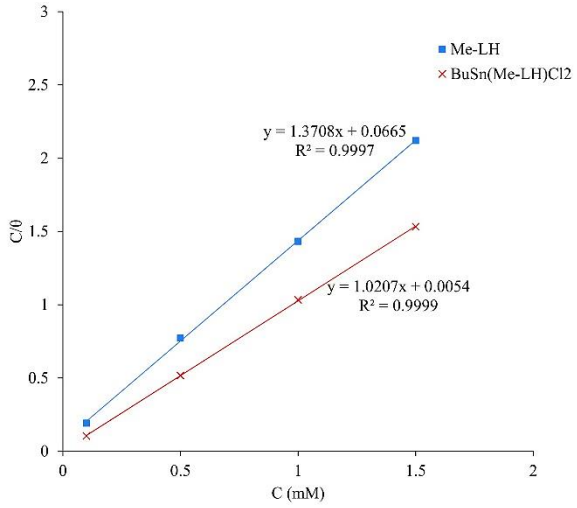

Figure 11 Langmuir isotherm for the adsorption of inhibitors using the polarisation method.

Mild steel surface morphology with and without Me-LH and BuSn(Me-LH)Cl$_2$ in HCl by SEM

The scanning electron micrographs of the mild steel surface in the presence and absence of inhibitors provided a better insight into the overall findings. The SEM micrographs of mild steel immersed in 1 M HCl for 24 h at 25 °C as affected by 1.5 mM inhibitors are shown in **Figures 12(a) - (d)**. **Figure 12(a)** shows an image of the freshly polished mild steel surface. **Figure 12(b)** shows the mild steel in the absence of inhibitor with the damaged surface due to the dissolution of metal in acidic solution. Some deep holes were found on the surface of mild steel which was related to pitting corrosion phenomenon [67]. Pitting marks on the surface was attributed to the effect of the aggressive acidic solution in the absence of inhibitors [68]. Nevertheless, **Figures 12(c)** and **12(d)** are the images of the inhibited mild steel surface which were immersed in a high concentration of inhibitors in 1 M acidic solution. The smoother surface of mild steel was noted as observed in **Figures 12(c)** and **12(d)** compared to that of mild steel without the presence of inhibitor **Figure 12(b)**. The observation could be explained by the reduction in the dissolution rate and the formation of a protective film that was adsorbed on the mild steel surface which prevented the aggressive acid attack [4]. Hence, in the presence of higher concentrations of inhibitor, there is no pitting observed and the complete surface coverage with the adsorbed Me-LH and BuSn(Me-LH)Cl$_2$ on the mild steel surfaces. On the other hand, the presence of

cracks on the protective film was reported to be induced during the surface dehydration step before the SEM imaging procedure [69]. Besides, some of the deposited particles were also found on the surface of mild steel which was possibly due to the multiple nucleations of the inhibitor as reported by Mohd *et al.* [70]. In an earlier study by Badr [71], when the adsorption density approaches the monolayer adsorption, the inhibitor molecules will slowly cover the nucleation sites and the entire surface of metal steel where inhibition occurs. The results proved that the surface of mild steel was adsorbed with inhibitors that contain nitrogen, sulfur, lone pairs of electrons and aromatic rings with delocalize π-electrons systems, hence protects the mild steel surface from corrosion attack. This finding is consistent with polarization and impedance results.

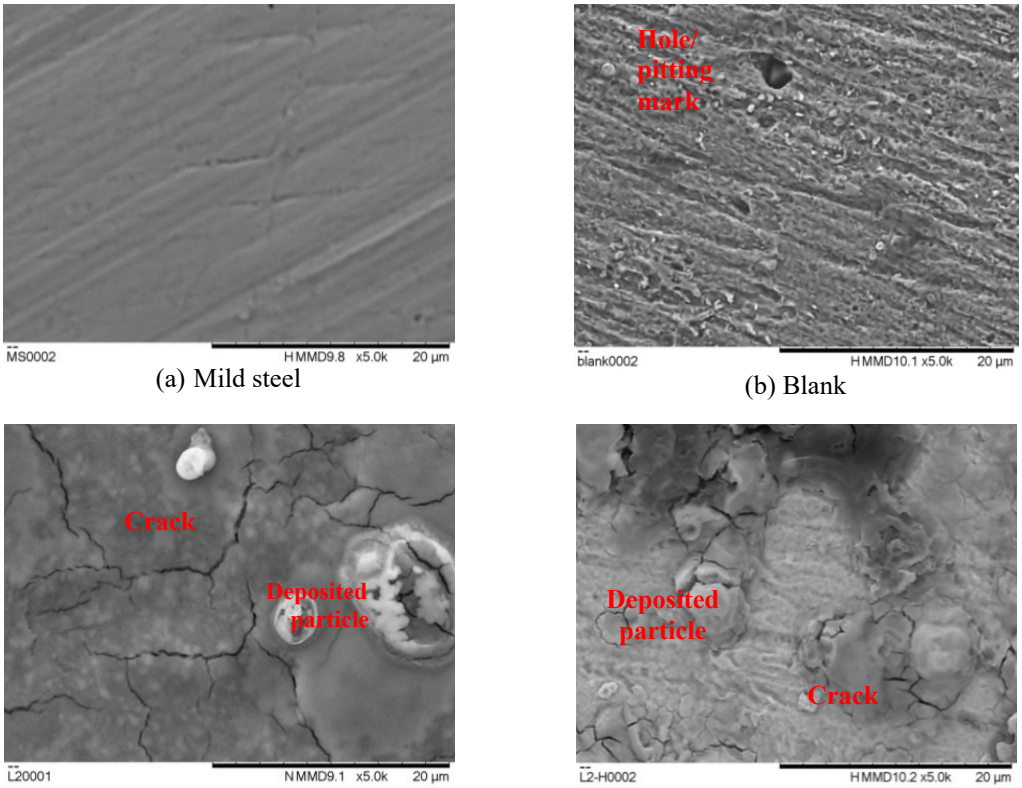

(a) Mild steel (b) Blank

(c) Me-LH (d) $BuSn(Me\text{-}LH)Cl_2$

Figure 12 SEM images of the mild steel surfaces in the presence and absence of inhibitors.

Conclusions

The Me-LH and $BuSn(Me\text{-}LH)Cl_2$ were successfully synthesised via the condensation process and direct method, respectively and were characterised using CHNS, FTIR, UV-Vis, molar conductivity, ^{1}H, ^{13}C, and ^{119}Sn NMR analyses. The findings showed that the ligand acts as a tridentate to the Sn(IV) ion that coordinates through the nitrogen atom and thiolate sulfur molecule. X-ray crystallographic analysis was also operated to confirm the molecular structure of compounds. The $BuSn(Me\text{-}LH)Cl_2$ was found to have a better inhibition efficiency compared to Me-LH. The inhibition efficiency results obtained using weight loss, EIS and Tafel polarization methods were not that comparable but the pattern of inhibition efficiency as affected by different levels of inhibitor concentration was noticeable. A similar trend was observed where an increment in the inhibition efficiency was noted with increasing concentration of inhibitor regardless of weight loss, EIS or Tafel polarization methods. The weight loss technique and electrochemical measurements were further confirmed with the SEM findings. The adsorption of the inhibitors on the mild steel surface in the 1 M HCl solution obeyed Langmuir adsorption isotherm and thermodynamic models. The negative sign of ΔG^{o}_{ads} suggested the occurrence of the spontaneous adsorption process. When inhibitors were applied into the 1 M HCl solution, an increment in the activation energy was noted indicative that chemisorption is more prevalent than physisorption.

Acknowledgements

The authors would like to express their gratitude to the Faculty of Applied Sciences, Universiti Teknologi MARA, Shah Alam Campus, Universiti Teknologi MARA Faculty of Applied Sciences, Negeri Sembilan Branch, Kuala Pilah Campus, for supporting research facilities. This project was funded by a research grant with the grant number FRGS/1/2016/STG01/UITM/03/6 from the Ministry of Higher Education. The funding period is between 2016 - 2018.

References

[1] MP Binsi, TK Joby, K Ragi, VC Sini and J Reeja. Interaction of two heterocyclic Schiff bases derived from 2-acetyl pyridine on mild steel in hydrochloric acid: Physicochemical and corrosion inhibition investigations. *Curr. Chem. Lett*. 2020; **9**, 19-30.

[2] NN Hazani, Y Mohd, SAIS Ghazali. Electrochemical studies of thiosemicarbazone derivative and its tin(IV) complex as corrosion inhibitor for mild steel in 1 M hydrochloric acid. *Chem. J. Mold*. 2019; **14**, 98-106.

[3] KF Khaled, OA Elhabib, A El-mghraby, OB Ibrahim and MAM Ibrahim. Inhibitive effect of thiosemicarbazone derivative on corrosion of mild steel in hydrochloric acid solution. *J. Mater. Environ. Sci.* 2010; **1**, 139-50.

[4] Y Meng, W Ning, B Xu, W Yang, K Zhang, Y Chen, L Li, X Liu, J Zheng and Y Zhang. Inhibition of mild steel corrosion in hydrochloric acid using two novel pyridine Schiff base derivatives: A comparative study of experimental and theoretical results. *RSC Adv.* 2017; **7**, 43014-29.

[5] AEAS Fouda, AAE Samir, HE Elsherbiny, AE Hazem and SA Ashraf. Experimental and surface morphological studies of corrosion inhibition on carbon steel in HCl solution using some new hydrazide derivatives. *RSC Adv.* 2021; **11**, 13497-512.

[6] A Dadgarinezhad and F Baghaei. A new synthesized corrosion inhibitor for mild steel in 0.5 M H_2SO_4. *Gazi Univ. J. Sci*. 2011; **24**, 219-26.

[7] S Kumar, H Vashisht, LO Olasunkanmi, I Bahadur, H Verma, G Singh, IB Obot and EE Ebenso. Experimental and theoretical studies on inhibition of mild steel corrosion by some synthesized polyurethane tri-block co-polymers. *Sci. Rep*. 2016; **6**, 1-18.

[8] P Mourya, S Banerjee, RB Rastogi and MM Singh. Inhibition of mild steel corrosion in hydrochloric and sulfuric acid media using a thiosemicarbazone derivative. *Ind. Eng. Chem. Res.* 2013; **52**, 12733-47.

[9] SV Sanap, RM Patil and RAMS Dubey. Corrosion inhibition of mild steel by using mixed ligand metal complexes. *Int. J. Chem. Sci.* 2013; **1**, 503-17.

[10] EA Florez-Frias, V Barba, R Lopez-Sesenes, LL Landeros-Martínez, JP Flores-De los Ríos, M Casales and JG Gonzalez-Rodriguez. Use of a metallic complex derived from *curcuma longa* as green corrosion inhibitor for carbon steel in sulfuric acid. *Int. J. Corros.* 2021; **2021**, 1-13.

[11] MH Mahross, K Efil, TAS El-nasr and OA Abbas. Experimental and theoretical study on corrosion inhibition of mild steel in oilfield formation water using some Schiff base metal complexes. *J. Electrochem. Sci. Technol*. 2017; **8**, 222-35.

[12] RB Rastogi, K Singh and JL Maurya. Synthesis and characterization of organotin(IV) thiobiurets. *Synth. React. Inorg. M.* 2012; **42**, 616-20.

[13] KL Rajesh and KS Amirthagadeswaran. Corrosion and wear behaviour of nano Al_2O_3 reinforced copper metal matrix composites synthesized by high energy ball milling. *Part. Sci. Technol*. 2019; 1-8.

[14] M Benabdellah, A Yahyi, A Dafali, A Aouniti, B Hammouti and A Ettouhami. Corrosion inhibition of steel in molar HCl by triphenyltin2-thiophene carboxylate. *Arab. J. Chem*. 2011; **4**, 243-47.

[15] H Kurniasih, M Nurissalam, B Iswantoro, H Afriyani, HI Qudus and S Hadi. The synthesis, characterization and comparative anticorrosion study of some organotin(IV) 4-chlorobenzoates. *Orient. J. Chem*. 2015; **31**, 2377-83.

[16] RB Rastogi, MM Singh, K Singh and M Yadav. Organotin dithiobiurets as corrosion inhibitors for mild steel-dimethyl sulfoxide containing HCl. *Afr. J. Pure Appl. Chem*. 2011; **5**, 19-33.

[17] S Hadi, H Afriyani, HI Qudus and Noviany. The anticorrosion activity of dibutyltin(IV) and diphenyltin(IV) dihydroxybenzoate compounds towards HRP mild steel in NaCl. *J. Chem. Pharm. Res.* 2016; **8**, 975-80.

[18] S Hadi, H Afriyani, DW Anggraini, IH Qudus and T Suhartati. Synthesis and potency study of some dibutyltin(IV) dinitrobenzoate compounds as corrosion inhibitor for mild steel HRP in DMSO-HCl solution. *Asian J. Chem*. 2015; **27**, 1509-12.

[19] Bruker. 2009. SMART, SAINT and SADABS. Bruker AXS, Madison, Wisconsin, USA.

[20] AL Spek. Structure validation in chemical crystallography. *Acta Cryst. D: Biol. Cryst*. 2009; **65**, 148-55.
[21] NN Hazani, NN Dzulkifli, SAISM Ghazali, Y Mohd, Y Farina and F Ngatiman. Synthesis, characterisation, crystal structure and anti-corrosion studies of an organotin (IV) complex of 2-acetylpyridine 4-ethyl-3- thiosemicarbazone (LH): N-BuSn (L)Cl_2. *ASM Sci. J.* 2019; **12**, 1-15.
[22] D Daoud, T Douadi, H Hamani, S Chafaa and M Al-noaimi. Corrosion inhibition of mild steel by two new *S*-heterocyclic compounds in 1 M HCl: Experimental and computational study. *Corros. Sci.* 2015; **94**, 21-37.
[23] M Muralisankar, R Sreedharan and S Sujith. *N*(1)-pentyl isatin-*N*(4)-methyl-*N*(4)-phenyl thiosemicarbazone (PITSc) as a corrosion inhibitor on mild steel in HCl. *J. Alloys Compd.* 2017; **695**, 171-82.
[24] NZN Hashim, K Kassim and Y Mohd. Corrosion inhibition of mild steel by *N*-phenyl-1,4-phenylenediamine and its Schiff base derivatives in 1 M HCl. *Adv. Mat. Res*. 2012; **554-556**, 408-13.
[25] A Paul, TK Joby, VP Raphael and KS Shaju. Electrochemical and gravimetric corrosion inhibition investigations of a heterocyclic Schiff base derived from 3-formylindole. *IOSR J. Appl. Chem.* 2012; **1**, 17-23.
[26] EE Ebenso, DA Isabirye and NO Eddy. Adsorption and quantum chemical studies on the inhibition potentials of some thiosemicarbazides for the corrosion of mild steel in acidic medium. *Int. J. Mol. Sci.* 2010; **11**, 2473-98.
[27] A Manivel, S Ramkumar, JJ Wu, AM Asiri and S Anandan. Exploration of (*S*)-4,5,6,7-tetrahydrobenzo[d]thiazole-2,6-diamine as feasible corrosion inhibitor for mild steel in acidic media. *J. Environ. Chem. Eng.* 2014; **2**, 463-70.
[28] SA Aly and SK Fathalla. Preparation, characterization of some transition metal complexes of hydrazone derivatives and their antibacterial and antioxidant activities. *Arab. J. Chem*. 2020; **13**, 3735-50.
[29] LNDA Neto, MDCAD Lima, JFD Oliveira, ERD Souza, MDS Buonafina, MNV Anjos, FA Brayner, LC Alves, RP Neves and FJB Mendonca-Junior. Synthesis, cytotoxicity and antifungal activity of 5-nitro-thiophene-thiosemicarbazones derivatives. *Chem. Biol. Interact.* 2017; **272**, 172-81.
[30] AQ Ali, SG Teoh, A Salhin and N Eltayeb. Synthesis of platinum(II) complexes of isatin thiosemicarbazones derivatives: In vitro anti-cancer and deoxyribosenucleic acid binding activities. *Inorganica Chim. Acta* 2014; **146**, 235-44.
[31] HP Ebrahimi, JS Hadi, TA Alsalim, TS Ghali and Z Bolandnazar. A novel series of thiosemicarbazone drugs: From synthesis to structure. *Spectrochim. Acta A Mol. Biomol. Spectrosc*. 2015; **137**, 1067-77.
[32] PP Netalkar, SP Netalkar and VK Revankar. Transition metal complexes of thiosemicarbazone: Synthesis, structures and invitro antimicrobial studies. *Polyhedron* 2015; **100**, 215-22.
[33] K Sampath, S Sathiyaraj, G Raja and C Jayabalakrishnan. Mixed ligand ruthenium(III) complexes of benzaldehyde 4-methyl-3-thiosemicarbazones with triphenylphosphine/triphenylarsine co-ligands: Synthesis, DNA binding, DNA cleavage, antioxidative and cytotoxic activity. *J. Mol. Struct.* 2013; **1046**, 82-91.
[34] YY Wu, YT Wang, YY Wang, MX Li, YL Lu and YH Zhang. Dimethyltin(IV) and palladium(II) complexes derived from 2-benzoylpyridine *N*(4)-cyclohexylthiosemicarbazone: Synthesis, crystal structures and biological evaluation. *Inorg. Chem. Commun.* 2017; **78**, 65-9.
[35] GL Parrilha, JG Da Silva, LF Gouveia, AK Gasparoto, RP Dias, WR Rocha, DA Santos, NL Speziali and H Beraldo. Pyridine-derived thiosemicarbazones and their tin(IV) complexes with antifungal activity against Candida spp. *Eur. J. Med. Chem.* 2011; **46**, 1473-82.
[36] MA Affan, FS Wan, Z Ngaini and M Shamsuddin. Synthesis, characterization and biological studies of organotin(IV) complexes of thiosemicarbazone ligand derived from pyruvic acid: X-ray crystal structure of [Me2Sn(PAT)]. *Malaysian J. Anal. Sci.* 2009; **13**, 63-72.
[37] K Venkatesh, P Rayam, KBC Sekhar and K Mukkanti. Synthesis, characterization and biological activity of some new thiosemicarbazide derivatives and their transition metal complexes. *Int. J. Appl. Biol. Pharm. Tech.* 2016; **7**, 258-67.
[38] MA Salam, MA Affan, R Saha, FB Ahmad and N Sam. Synthesis, characterization and in vitro antibacterial studies of organotin(IV) complexes with 2-hydroxyacetophenone-2-methylphenylthiosemicarbazone (H2dampt). *Bioinorg. Chem. Appl.* 2012; **2012**, 1-9.
[39] SA Hosseini-Yazdi, S Hosseinpour, AA Khandar and J White. Synthesis, characterization, and X-ray crystal structures of copper(II) and nickel(II) complexes with two bis(thiosemicarbazone) ligands and investigation of their electrochemical behavior. *Transit. Met. Chem.* 2016; **41**, 65-75.

[40] SA Hosseini-Yazdi, S Hosseinpour, AA Khandar, WS Kassel and NA Piro. Copper(II) and nickel(II) complexes with two new bis(thiosemicarbazone) ligands: Synthesis, characterization, X-ray crystal structures and their electrochemistry behavior. *Inorganica Chim. Acta.* 2015; **427**, 124-30.

[41] O Abdalla, Y Farina and N Ibrahim. Synthesis, characterization and antibacterial study of copper(II) complexes of thiosemicarbazones. *Malaysian J. Anal. Sci.* 2015; **19**, 1171-8.

[42] HL Singh, JB Singh and KP Sharma. Synthetic, structural, and antimicrobial studies of organotin(IV) complexes of semicarbazone, thiosemicarbazone derived from 4-hydroxy-3-methoxybenzaldehyde. *Res. Chem. Intermed.* 2012; **38**, 53-65.

[43] S Wang, QL Li, RF Zhang, JY Du, YX Li and CL Ma. Novel organotin(IV) complexes derived from 4-carboxybenzenesulfonamide: Synthesis, structure and in vitro cytostatic activity evaluation. *Polyhedron* 2019; **158**, 15-24.

[44] DG Calatayud, E López-Torres, MA Mendiola and JR Procopio. Tin(IV) complexes with thiosemicarbazide and 4-methyl-3-thiosemicarbazide derivatives. *Z. Anorg. Allg. Chem.* 2007; **633**, 1925-31.

[45] N Khan, Y Farina, LK Mun, NF Rajab and N Awang. Syntheses, characterization, X-ray diffraction studies and in vitro antitumor activities of diorganotin(IV) derivatives of bis(*p*-substituted-*N*-methylbenzylaminedithiocarbamates). *Polyhedron* 2015; **85**, 754-760.

[46] W Rehman, MK Baloch and A Badshah. Synthesis, spectral characterization and bio-analysis of some organotin(IV) complexes. *Eur. J. Med. Chem.* 2008; **43**, 2380-85.

[47] AD Khalaji, G Grivani, SJ Akerdi, K Gotoh, H Ishida and H Mighani. Synthesis, spectroscopic characterization, crystal structures, and theoretical studies of (E)-2-(2,4-dimethoxybenzylidene) thiosemicarbazone and (E)-2-(2,5-dimethoxybenzylidene)thiosemicarbazone. *Struct. Chem.* 2010; **21**, 995-1003.

[48] MA Affan, MA Salam, FB Ahmad, F White and HM Ali. Organotin(IV) complexes of 2-hydroxyacetophenone-*N*(4)-cyclohexylthiosemicarbazone (H2dact): Synthesis, spectral characterization, crystal structure and biological studies. *Inorganica Chim. Acta.* 2012; **387**, 219-25.

[49] MHSA Hamid, ANAH Said, AH Mirza, MR Karim, M Arifuzzaman, MA Ali and PV Bernhardt. Synthesis, structures and spectroscopic properties of some tin(IV) complexes of the 2-acetylpyrazine Schiff bases of S-methyl- and S-benzyldithiocarbazates. *Inorganica Chim. Acta*. 2016; **453**, 742-50.

[50] MX Li, D Zhang, LZ Zhang, JY Niu and BS Ji. Diorganotin(IV) complexes with 2-benzoylpyridine and 2-acetylpyrazine *N*(4)-phenylthiosemicarbazones: Synthesis, crystal structures and biological activities. *J. Organomet. Chem.* 2011; **696**, 852-8.

[51] A Pérez-Rebolledo, GM de Lima, NL Speziali, OE Piro, EE Castellano, JD Ardisson and H Beraldo. Tin(IV) complexes obtained by reacting 2-benzoylpyridine-derived thiosemicarbazones with $SnCl_4$ and Ph_2SnCl_2. *J. Organomet. Chem*. 2006; **691**, 3919-30.

[52] SR Batten. Structural and spectral studies of a new copper(II) complex with a tridentate thiosemicarbazone ligand. *Struct. Chem.* 2008; **9**, 137-42.

[53] H Keles, DM Emir and M Keles. A comparative study of the corrosion inhibition of low carbon steel in HCl solution by an imine compound and its cobalt complex. *Corros. Sci.* 2015; **101**, 19-31.

[54] NZN Hashim, K Kassim and Y Mohd. (*E*)-*N*1-(4-chlorobenzylidene)-*N*4-phenylbenzene-1,4-diamine as mild steel corrosion inhibitor in 1 M HCl. *APCBEE Procedia*. 2012; **3**, 239-44.

[55] KS Jacob and G Parameswaran. Corrosion inhibition of mild steel in hydrochloric acid solution by Schiff base furoin thiosemicarbazone. *Corros. Sci.* 2010; **52**, 224-8.

[56] FM Mahgoub and SM Al-Rashdi. Investigate the corrosion inhibition of mild steel in sulfuric acid solution by thiosemicarbazide. *Open J. Phys. Chem*. 2016; **6**, 54-66.

[57] TI Kashar, M Abdel-Motaal, K Emran and NA Sukar. Preparation and characterization of thiosemicarbazones corrosion inhibition effect and the antimicrobial and anticancer effect on their metal complexes. *Eur. Sci. J*. 2017; **13**, 249-78.

[58] B Xu, W Yang, Y Liu, X Yin, W Gong and Y Chen. Experimental and theoretical evaluation of two pyridinecarboxaldehyde thiosemicarbazone compounds as corrosion inhibitors for mild steel in hydrochloric acid solution. *Corros. Sci.* 2014; **78**, 260-8.

[59] DB Hmamou, R Salghi, A Zarrouk, H Zarrok, R Touzani, B Hammouti and AE Assyry. Investigation of corrosion inhibition of carbon steel in 0.5 M H_2SO_4 by new bipyrazole derivative using experimental and theoretical approaches. *J. Environ. Chem. Eng*. 2015; **3**, 2031-41.

[60] CG Dariva and AF Galio. *Corrosion inhibitors - principles, mechanisms and applications*. *In:* M Aliofkhazraei (Ed.). Developments in corrosion protection. IntechOpen, London, 2014, p. 710.

[61] AM Al-Bonayan. Inhibiting effect of thiosemicarbazide and 4-phenyl thiosemicarbazide towards the corrosion of carbon steel in H_3PO_4 solutions. *Int. J. Electrochem. Sci*. 2015; **10**, 589-601.
[62] S Chitra, K Parameswari, C Sivakami and A Selvaraj. Sulpha Schiff bases as corrosion inhibitors for mild steel in 1 M sulphuric acid. *Chem. Eng. Res. Bull.* 2010; **14**, 1-6.
[63] M Prajila, J Sam, J Bincy and J Abraham. Electroanalytical studies on the interaction of 4-(*N*,*N*-dimethylaminobenzilidine)-3-mercapto-6-methyl-1, 2, 4-triazin (4H)-5-one (DAMMT) with mild steel in perchloric acid. *J. Mater. Environ. Sci.* 2012; **3**, 1045-64.
[64] C Verma, MA Quraishi, K Kluza, M Makowska-Janusik, LO Olasunkanmi and EE Ebenso. Corrosion inhibition of mild steel in 1 M HCl by *D*-glucose derivatives of dihydropyrido [2,3-d:6,5-d′] dipyrimidine-2, 4, 6, 8(1H,3H, 5H,7H)-tetraone. *Sci. Rep*. 2017; **7**, 1-17.
[65] H Zarrok, H Oudda and A Zarrouk. Weight loss measurement and theoretical study of new pyridazine compound as corrosion inhibitor for C38 steel in hydrochloric acid solution. *Der Pharma Chem.* 2011; **3**, 576-90.
[66] MR Vinutha and TV Venkatesha. Review on mechanistic action of inhibitors on steel corrosion in acidic media. *Port. Electrochim. Acta* 2016; **34**, 157-84.
[67] Z Zhan, M Sun, Y Jiang, L Li and J Li. Effect of tin on the corrosion resistance of 16 Cr ferritic stainless steel in acidic solution and chloride-containing media. *Int. J. Electrochem. Sci.* 2016; **11**, 3963-75.
[68] G Khan, WJ Basirun, SN Kazi, P Ahmed, L Magaji, SM Ahmed, GM Khan and MA Rehman. Electrochemical investigation on the corrosion inhibition of mild steel by quinazoline Schiff base compounds in hydrochloric acid solution. *J. Colloid Interface Sci.* 2017; **502**, 134-45.
[69] AAH Kadhum, AB Mohamad, LA Hammed, AA Al-Amiery, NH San and AY Musa. Inhibition of mild steel corrosion in hydrochloric acid solution by new coumarin. *Mater.* 2014; **7**, 4335-48.
[70] NK Mohd, MJ Ghazali, YS Kian, NA Ibrahim, WMZWS Yunus, MM Nor and Z Idris. Corrosion inhibitor of mild steel in hydrochloric acid solution using fatty acid derivatives. *J. Oil Palm Res.* 2017; **29**, 97-109.
[71] GE Badr. The role of some thiosemicarbazide derivatives as corrosion inhibitors for C-steel in acidic media. *Corros. Sci.* 2009; **51**, 2529-36.